THE ARCHIVE OF MECHANICAL ENGINEERING

Vol. XLIX 2002 Number 1

Key words: *transonic flows, nonstationary airfoil loading*

WITOLD C. SELEROWICZ[*)]

THE EFFECT OF AIR HUMIDITY ON OSCILLATORY AIRFOIL FLOW

The effect of air humidity on oscillatory flow around the NACA 0012 airfoil was investigated experimentally at Mach number M=0.71 and airfoil angle of attack α=8.5°. The background flow oscillations were produced by a rotating rectangular plate placed downstream of the airfoil. The generated oscillation frequencies were in the range from 0.5 up to 1.5 of the buffet frequency. The presented results shown that the normal aerodynamic force variations strongly depend on the excitation frequency and reach a maximum value at frequencies typical to the buffet. The increase of the air humidity leads to considerable diminishing of the aerodynamic force variation.

1. Introduction

Transonic airfoil flow with shock waves can produce series of instabilities and, in consequence, leads to unsteady airfoil loading. This phenomenon have been studied experimentally for more then twenty years [1], [2], [3], [4], [5], [6], [7], [8].

However, apart from self-excited instabilities sustained in steady background flow conditions, there exist flow regimes in which the airfoil instabilities can be additionally affected by periodic acceleration and deceleration of the background flow. This is, for example, the flow around the helicopter rotor blade, where the flow velocity, as well the blade angle of attack, periodically change during each rotor revolution [9], [10], [11]. Most of the experimental investigations concerning the unsteady flow on a airfoil were performed by periodic changing the airfoil angle of attack, whereas the background flow was kept constant [12], [14], [15], [16], [17], [18].

Another possibility is a flow around a fixed airfoil in presence of periodic variations of the background flow velocity. Due to the complicated way of

[*)] *Warsaw University of Technology, Institute of Aeronautics and Applied Mechanics, ul. Nowowiejska 24, 00-665 Warsaw, Poland; E-mail: seler@meil.pw.edu.pl*

realisation of such a flow conditions in a transonic tunnel, the number of experimental works is considerably smaller. In a visualisation study [19], the self-excited oscillations on the NACA 0012 airfoil at steady transonic background flow (M_∞=0.7) were compared with the periodically changing flow at frequencies close to the buffet frequency. It had been found that, in the acceleration flow phase, the length of the separation region decreases, whereas it increases in the deceleration phase. The airfoil loading itself was the object of interest in another experimental work [20], where the influence of the background excitation frequency on the separation process at low and high angle of attack was the subject of interest. Frequencies of the background flow oscillations under consideration were in the range from 0.5 up to 1.0 of the buffet frequency.

Both of the mentioned experimental study were performed at only one air humidity. On the other hand, it is well know that, in the case of self-excited oscillations, the increase of air humidity leads to reduction of the unsteady effects. So, the main aim of the present work was to find the quantitative relation between the non-stationary airfoil loading and the air humidity.

2. Experimental set-up

All measurements were performed in a short operating time transonic wind tunnel (Fig. 1). The mean velocity of the flow was stabilised by the regulating valve which controlled the choked flow from the container at atmospheric pressure to the vacuum vessel. The use of the flexible container having a volume of approximately 50 m^3 allowed for precise preparation of the inlet air

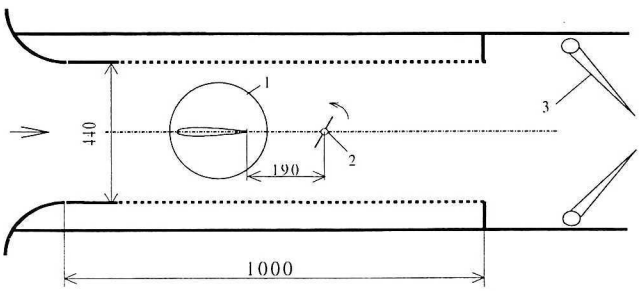

Fig. 1 Scheme of the transonic wind tunnel test section: 1 – glass window mounted for flow visualisation, 2 – rotating plate, 3 – adjusting valve

temperature and humidity. In the presented experiments, the air temperature in the container was kept constant at 22°C, and decreased downstream up to -4°C in the tunnel test section. The initial relative air humidity was changed in four steps: 12, 40, 60 and 80%. In the tunnel test section, the relative air humidity increased in the first case up to 40%, whereas in the second one it reached the value of 100%. In the last two cases, the situation was more complicated,

because the initial moisture content led, after expansion to the test section conditions, to overcooling vapour conditions. Due to the short time of the expansion process, the condensation of the main stream was not observed in the test section. The process of condensation was observed only on the upper airfoil surface in some phases of flow oscillation, as it will be shown in chapter 3.2.

The symmetric NACA0012 airfoil with 120 mm chord length and 100 mm width was located in the tunnel test section. The airfoil angle of attack was kept constant at $\alpha=8.5^{\circ}$ in all measurements, as it was done in [19] and [20]. The tunnel flow was periodically modified by an aerodynamic generator in the form of a rotating plate having the dimensions 40×100 mm. The plate was located downstream of the airfoil, 190 mm from its trailing edge (Fig. 1). The change in the plate rotation rate made it possible to achieve the range of excitation frequency from 78 to 240 Hz. The calculated excitation parameter $n_e=f_ec/U$ based on the excitation frequency f_e, airfoil chord length c, and tunnel average flow velocity U varied from 0.04 up to 0.12. The Reynolds number based on the average tunnel velocity and chord length was $2\cdot10^6$.

The change of the mean parameters of the tunnel flow was controlled by a reference pressure transducer Kulite XCS093. It was mounted at the side wall of the test section at 140 mm distance from the airfoil leading edge (Fig. 2).

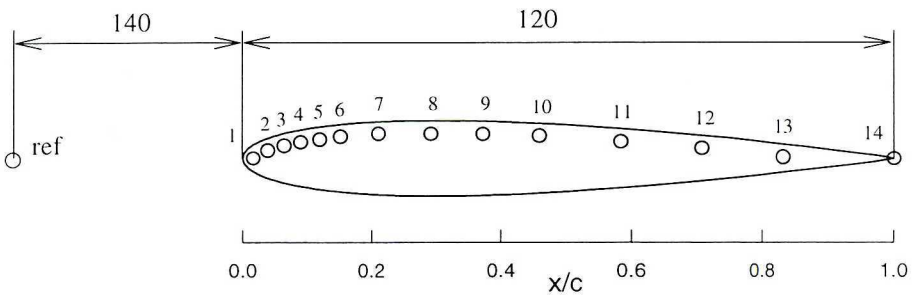

Fig. 2 Distribution of pressure transducers along the airfoil

In all experiments two identical NACA0012 airfoils were used. One of them was specially prepared for pressure measurements by assembling a set of 13 XCS093 miniature Kulite transducers (see Fig. 2). They were mounted inside the airfoil in its symmetry plane on the suction surface. An additional pressure transducer (number 14) was placed on the tunnel side-wall near the airfoil trailing edge. To realise pressure measurements on the airfoil bottom surface, the airfoil was mounted upside down and the rotation of the plate was turned round. This all was possible owing to the symmetry of the NACA 0012 airfoil.

During the flow visualisation, another NACA0012 airfoil was mounted between two glass windows of 230 mm diameter.

Pressure traces from the reference pressure transducer and their frequency spectra obtained at low, middle and high excitation frequency in a tunnel

without airfoil are shown in Fig. 3. As it can be seen, the pressure signal corresponding to the lowest excitation frequency (78 Hz) is characterised by one distinct spectral line, whereas in the other spectra higher frequency components are visible. However, due to their low amplitudes in comparison with the base spectrum component, all presented pressure variations can be considered as nearly harmonic.

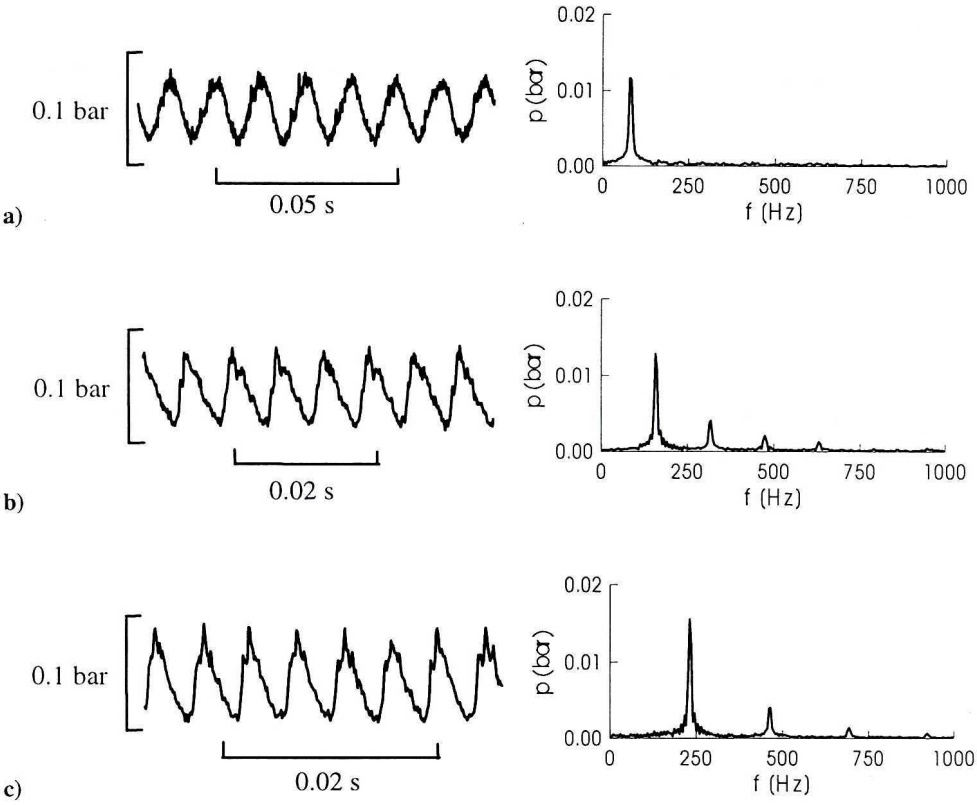

Fig. 3 Pressure histories at reference point and their frequency spectra for various excitation frequencies: a) 78 Hz, b) 156 Hz, c) 230 Hz

Variations of the tunnel Mach number at the reference point are shown in Fig. 4 for various air humidity levels. The Mach number is drawn versus excitation parameter n_e. It can be noted that the average Mach number remains constant and equal to approximately M=0.71, irrespective of the excitation frequency and air humidity. The range of Mach number variations attains a value of $\Delta M = M_{max} - M_{min} = 0.085$ at the lowest oscillation frequency (n_e=0.04) and increases up to $\Delta M = 0.13$ at n_e=0.12. The unlikeness of the tunnel Mach number due to the variation in air humidity appeared lower then 0.006 for M_{avg} and reached a value of 0.015 for M_{min} and M_{max}.

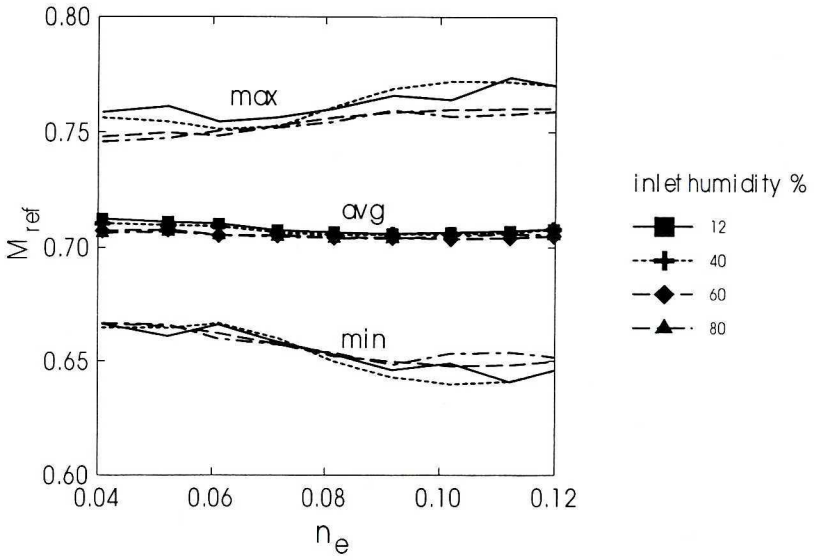

Fig. 4 Average, maximum and minimum Mach number at reference point versus excitation parameter

3. Results

3.1. Airfoil pressure distribution

Pressure traces obtained at the selected points on the airfoil are presented in Fig. 5. The signals were recorded at low, middle and high excitation frequency on the suction airfoil side, and are presented in the left column for the case of dry air and in the right column for the humid air. It is noticeable that, in all considered cases, the amplitudes of the signals are not uniformly distributed along the airfoil surface, and reach their highest amplitudes in the middle part of the airfoil. With the exception of Fig.5a, the signals are very regular in this region. In the rear part of the airfoil, all of the signals confirm the turbulent character of the flow. As mentioned above, at low excitation frequency and dry air, the signals obtained in the middle part of the airfoil are not regular (Fig. 5a). This is due to the complex flow structure over the airfoil, consisting of a self-excited shock oscillation and an oscillation of background flow.

RMS values of pressure pulsation along the cord length are shown in Fig. 6 for dry (a) and humid (b) air to present the influence of the excitation frequency on pressure pulsation distribution. All values are normalised by the corresponding RMS values at reference point (see Fig. 2). From both figures it can be seen that first of all, amplitudes of pressure pulsations on the upper (suction) side are much greater then on the bottom (pressure) side. On the

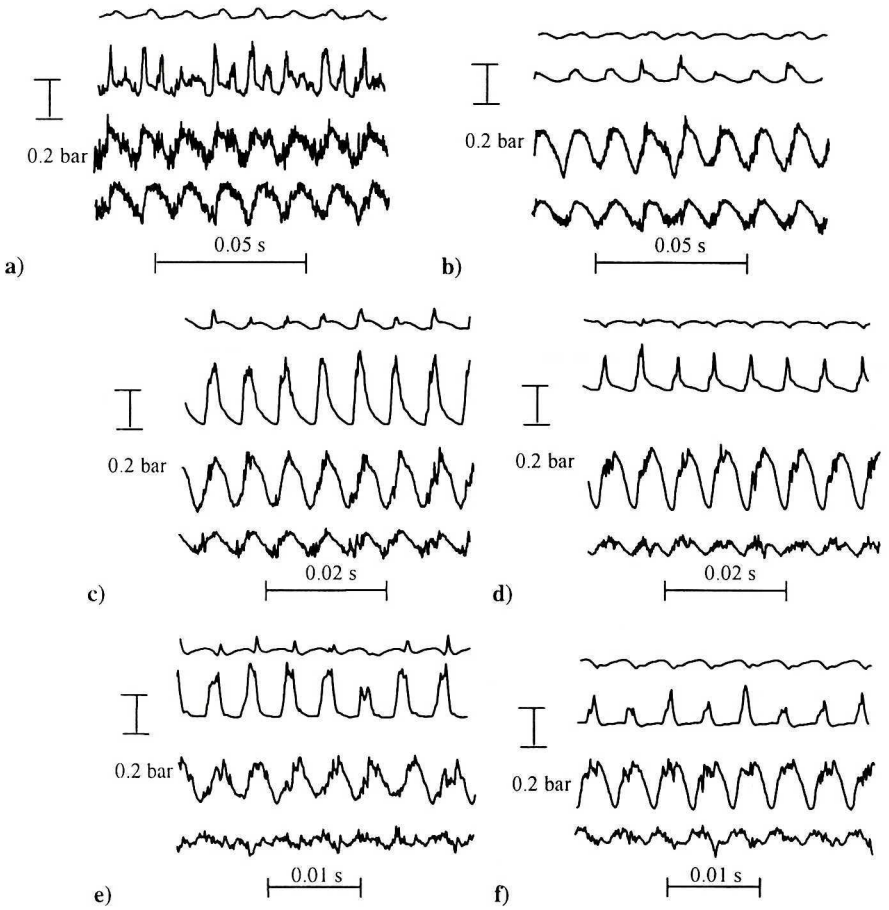

Fig. 5 Pressure histories at selected positions on the top and bottom airfoil surface for dry (inlet humidity H=12% – left column) and humid air (inlet humidity H=80% – right column). The x/c values for traces 1÷4 are: 0.034; 0.15; 0.46 and 0.84. The excitation frequencies are: 78 Hz (a,b), 156 Hz (c,d) and 230 Hz (e,f)

bottom surface, RMS levels near the leading edge are of the same order as at the reference point, and slightly increase downstream, nearly independent of air humidity. In contrast, the RMS values of pressure pulsations on the upper airfoil side depend on both the excitation frequency and air humidity. For dry air (Fig. 6a), pressure pulsations increase rapidly at the initial part of the airfoil and then decrease (with the exception of the low excitation frequency). They reach maximum values at x/c=0.2, and are many times greater than value characteristic for the freestream flow. At excitation frequency close to the buffet frequency (156 Hz, n_e=0.08), the $p'_{RMS}/p'_{RMS}(ref)$ exceeds a value of approximately 7. At low excitation frequency (78 Hz), the distribution of RMS pressure pulsation differs from recorded at the highest frequencies, and also shows significant increase in the rear part of the airfoil.

Distributions of RMS pressure pulsation obtained in humid air (Fig. 6b) show significant differences in comparison with those for dry air (Fig. 6a). The shape of the distribution is characterised by two clearly visible maxima. One of them is located at x/c=0.2, whereas the second one, with a higher amplitude, exists at x/c=0.4. At middle and high excitation frequencies, the values of RMS are lower than those obtained in dry air. At low excitation frequency, the relation is opposite.

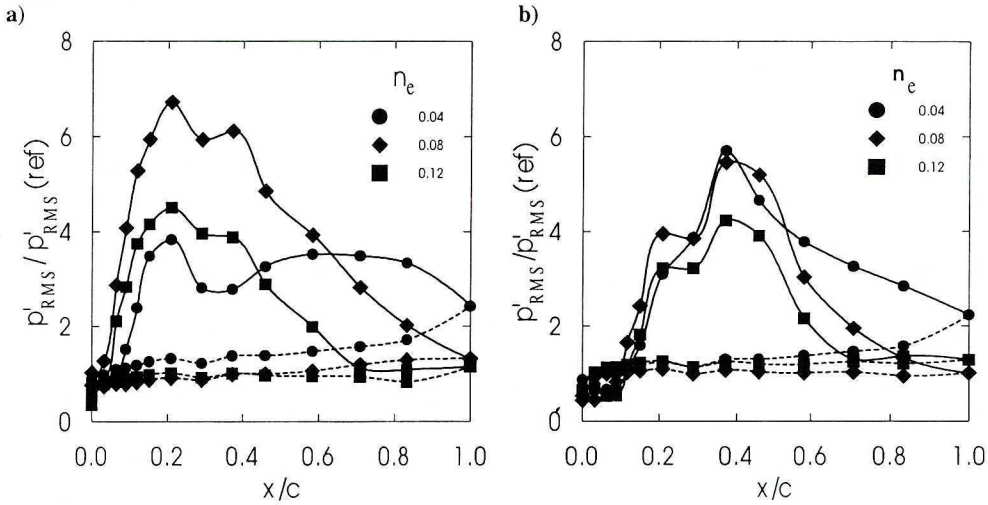

Fig. 6 Normalised RMS values of pressure variations along the top (continuous lines) and bottom (dashed lines) airfoil surface: a) inlet humidity H=12%, b) inlet humidity H=80%

3.2. Momentary airfoil loading

From pressure signals recorded on both airfoil sides, momentary pressure distributions were reconstructed. The non-dimensional pressure coefficient was determined using the following formula

$$C_p = \frac{\frac{p(t)}{\overline{p_{ref}}} - 1}{\frac{1}{2} k \overline{M_{ref}}^2},$$

where: C_p – pressure coefficient,

$p(t)$ – time depending pressure on the airfoil surface,

$\overline{p_{ref}}$ – time averaged pressure at the reference point,

$\overline{M_{ref}}$ – time averaged Mach number at the reference point (calculated from the isentropic formula),

k – isentropic exponent.

The integration time used for the calculation of $\overline{p_{ref}}$ and $\overline{M_{ref}}$ was greater than ten cycles of baseflow oscillation in each case.

Momentary C_p distributions representing a set of phases from one cycle of baseflow oscillation are shown in Fig. 7 for both dry and humid air (continuous and dashed lines, respectively). The excitation frequency f=156 Hz (n_e=0.08) corresponding to the buffet frequency at M=0.71 and α=8.5° is the same in both cases.

In the first flow phase (minimal value of M_{ref} – Fig. 7a) both pressure distributions indicate full separation on the top airfoil surface. For dry air, the separation region begins a little earlier than for the humid air. The separation bubble, which can be identified at x/c=0.6, seems to be less intensive than for humid air.

In the next flow phase, a shock existing on the suction airfoil side intensifies and moves towards the trailing edge with increasing M_{ref}. The negative pressure region (Fig. 7b, c) increases faster in the case of humid air than in the case of dry air, where the full separation conditions remain a little longer. Unfortunately, due to the limited number of pressure transducers and the complicated shape of the lambda shock wave near the airfoil surface, its position cannot be exactly established. In the subsequent flow phase (Fig. 7d,e), pressure distributions show nearly the same shapes, but the negative values of the pressure coefficient are higher for dry air. Such a situation remains also in the flow phase corresponding to the maximum value of the reference flow Mach number (Fig. 7f). At this stage, both the negative C_p values on the suction surface and the total C_n force (see next chapter) are maximal. The comparison of both pressure distributions presented in this figure shows that the C_n force should be slightly greater for dry air then for humid air.

With the decrease of the reference Mach number, the shock moves upstream toward the leading edge (Fig. 7g,h). In this flow phase, one can noticed large differences in pressure distributions between the case of dry and humid air. Distributions shown in Fig. 7h,i indicate fully developed flow separation in the case of dry air, whereas for humid air, the flow is not separated. In the final stage of oscillation (Fig. 7j), the flow on the airfoil is separated in both cases, although for humid air higher negative C_p values are visible. This indicates that the C_n value for a dry air flow must be lower than for humid air.

It seems to be distinctive that C_p distributions on the bottom airfoil surface show much smaller dependence on the humidity level of air. Thus, the influence of the bottom surface on the changes of C_n force is less essential.

Schlieren photographs at flow instants corresponding to the extreme shock wave positions on the airfoil top side are shown in Fig. 8a,c for dry and in Fig. 8b,d for humid air. As it can be seen, in the flow phase which corresponds to the total flow separation (a,b), small shocklets on the suction surface near the edge of the attack are present in both cases.

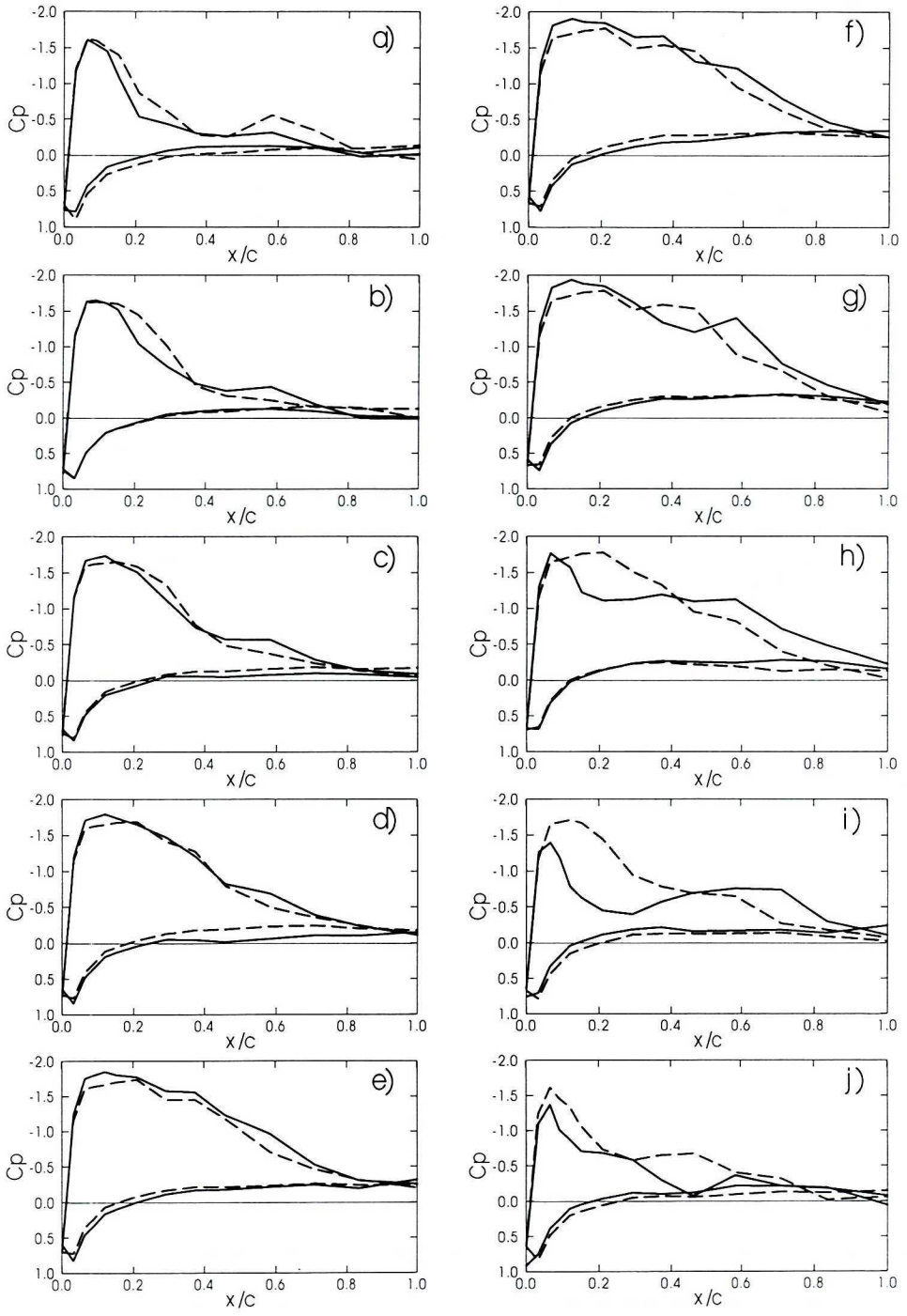

Fig. 7 Momentary pressure distributions on the top and bottom airfoil surface for dry (inlet humidity H=12% – continuous lines) and humid air (inlet humidity H=80% – dashed lines). The excitation frequency is 156 Hz

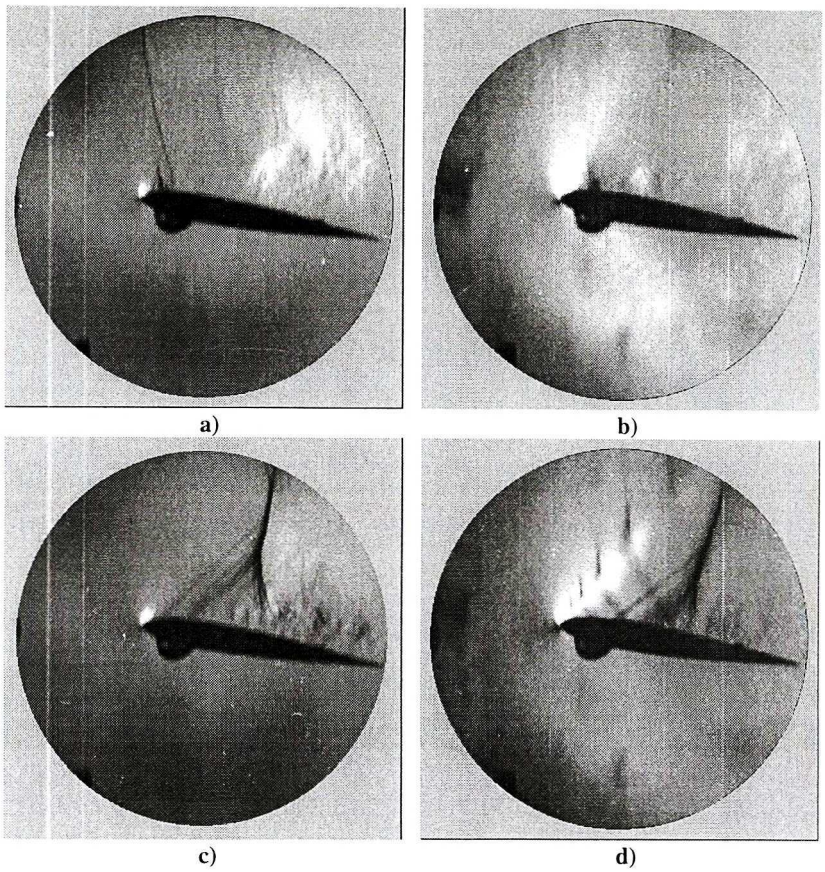

Fig. 8 Schlieren photographs of airfoil flow at M_{ref}=min (a,b) and M_{ref}=max (c,d) for dry (inlet humidity H=12% - left column) and humid air (inlet humidity H=80% - right column)

However, in the flow phase corresponding to the maximum C_n values (c,d), the flow is characterised by strong shocks of lambda type with succeeding flow separation. It can be noticed that in the case of humid air, the shock is located closer to the training edge than for dry air. In this case, the shock is, in addition, preceded by a few distinct condensation waves located in the acceleration region of the airfoil (Fig. 8d).

Temporary pressure distributions on the suction and pressure airfoil surfaces, corresponding to minimal and maximal excitation frequency under consideration, are shown in Fig. 9a,b (f=78 Hz, n_e=0.04) and Fig. 9c,d (f=230 Hz, n_e=0.12). As before, C_p distributions for dry and humid air are compared. Fig. 9a shows that in flow phase corresponding to maximum value of the M_{ref} the C_p distributions show some differences. It is due to the fact that in the case of low excitation frequency, two different forms of oscillation occur simultaneously on the airfoil. One of them corresponds to externally excited background flow, whereas the second one is self-excited (buffet). This is especially visible for dry air, and is confirmed by C_n spectrum shown in Fig. 11a.

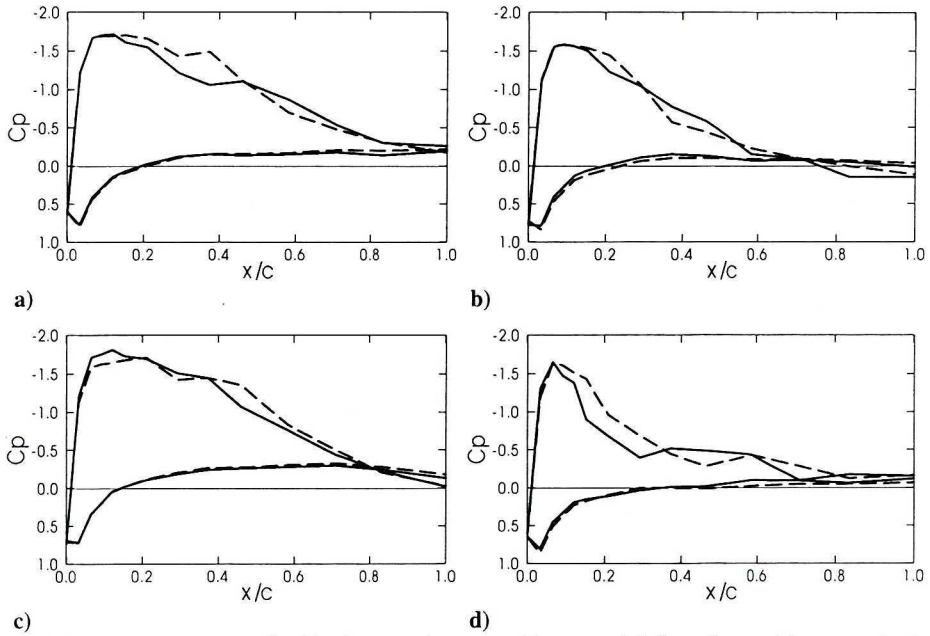

Fig. 9 Momentary pressure distributions on the top and bottom airfoil surface at M_{ref}=max (a,c) and M_{ref}=min (b,d) for dry (inlet humidity H=12% - continuous lines) and humid air (inlet humidity H=80% - dashed lines). Excitation frequencies are: 78 Hz (a,b) and 230 Hz (c,d)

Momentary pressure distributions obtained by the maximum value of n_e in phase of max M_{ref} (Fig. 9c) have nearly the same shape as in the case of minimum excitation frequency (Fig. 9a). In the phase of minimum M_{ref} (Fig. 9d), the separation region in the case of dry air is wider than in the case of humid air.

3.3. Aerodynamic force coefficient

Pressure distributions showed in Chapter 3.2 facilitated the calculation of the aerodynamic force coefficient following the formula

$$C_n(t) = \int_0^1 \left(C_{p_b} - C_{p_u}\right) d(x/c),$$

where: $C_n(t)$ – time depending aerodynamic force coefficient,

C_{p_b} – temporary pressure coefficient at the bottom airfoil surface,

C_{p_u} – temporary pressure coefficient at the upper airfoil surface,

x/c – non-dimensional cord length.

Results received for five various excitations are presented in Fig. 10a,c,e,g,i for dry air (inlet humidity H=12% – left column) and in Fig. 10b, d, f, h, j for humid air (inlet humidity H=80% – right column). The corresponding spectra of C_n are shown in Fig. 11a–11j.

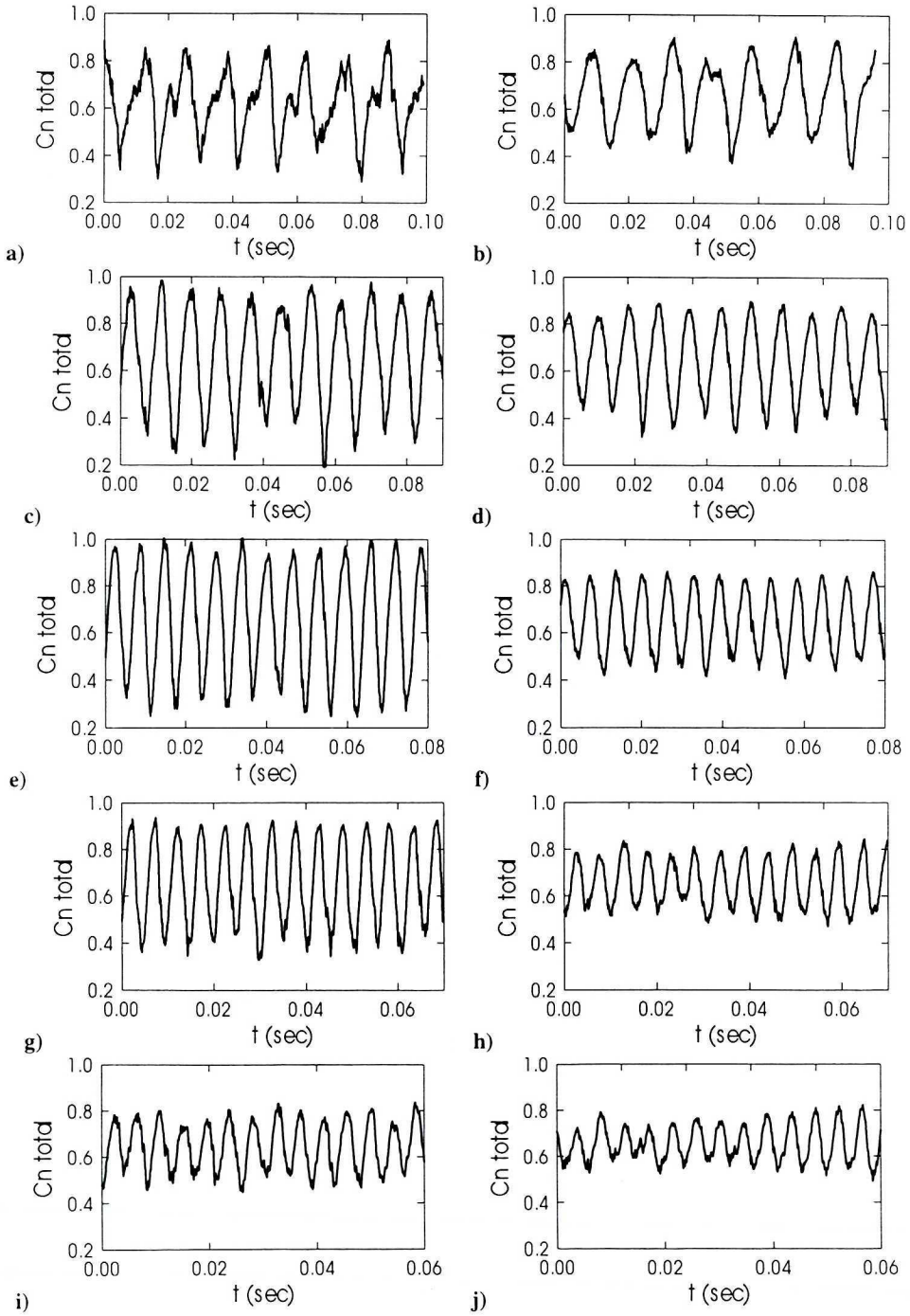

Fig. 10 Time histories of normal aerodynamic force coefficient C_n for dry (inlet humidity H=12% – left column) and humid air (inlet humidity H=80% – right column). Excitation frequencies are: 78 Hz (a,b), 117 Hz (c,d), 156 Hz (e,f), 195 Hz (g,h), 230 Hz (i,j)

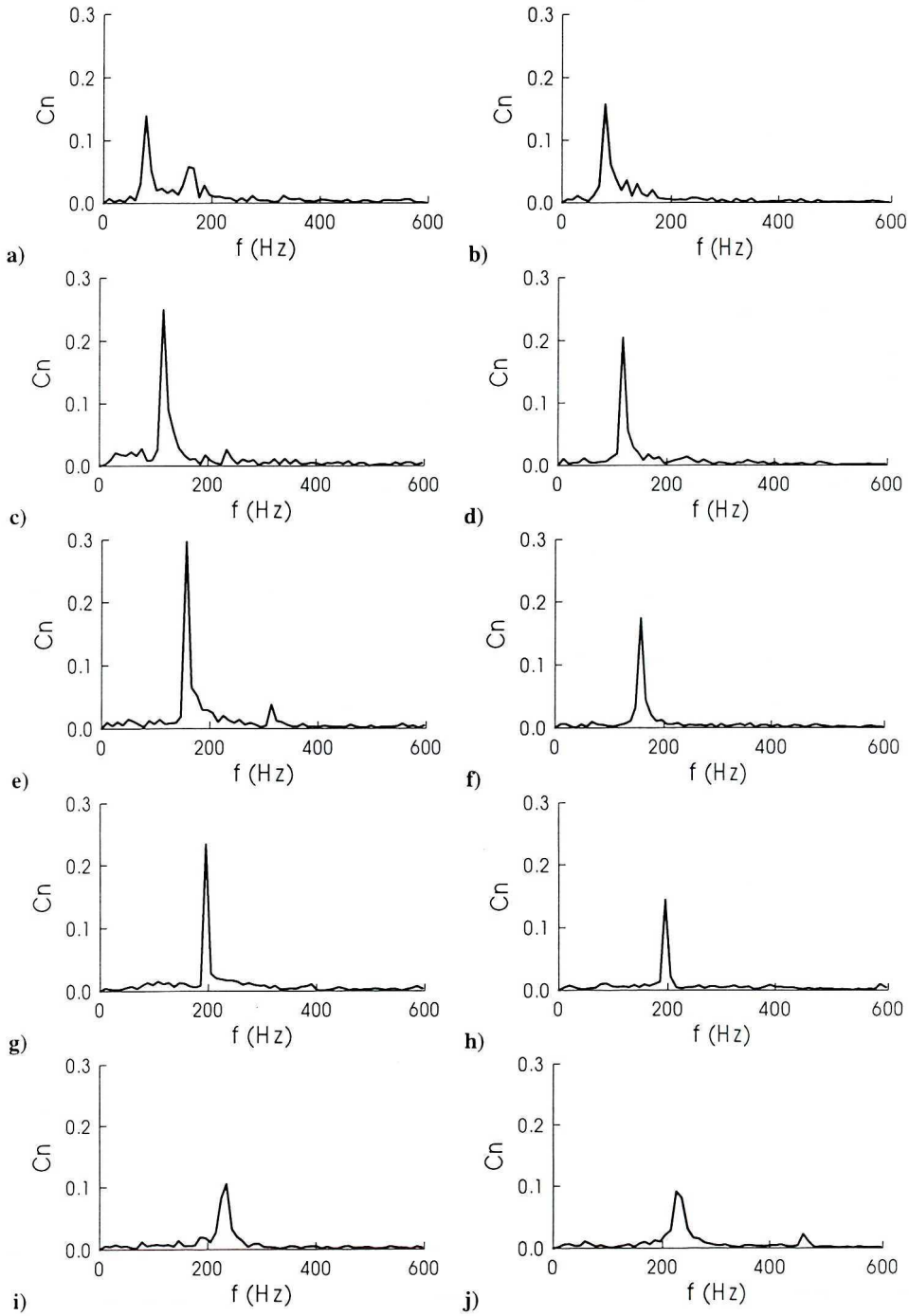

Fig. 11 Spectra of normal aerodynamic force coefficient C_n (for description see previous figure)

As it can be deduced from Fig. 10a, the $C_n(t)$ trace shows a rather irregular shape at low excitation frequency. In the frequency spectrum (Fig. 11a) there exists, apart from a peak representing the frequency of excitation (f=78 Hz), another peak of approximately f=160 Hz corresponding to the buffet frequency. With the increasing of the excitation frequency (Fig. 10c), the amplitude of the C_n oscillation increases and the frequency spectrum (Fig. 11c) has only one discrete component. This gives the indication that the airfoil flow is now fully dominated by the forced oscillation. As it has been expected, when the excitation frequency comes closer to the buffet frequency (f=156 Hz – Fig. 10e), the C_n oscillation achieves its maximum. The difference between the maximum and the minimum value $\Delta C_n = C_{n(max)} - C_{n(min)}$ is of the same order as the C_n time-average value. In the frequency spectrum (Fig.11e), a new peak representing the second harmonic becomes visible.

For the excitation frequency higher than the buffet frequency, a slow diminishing of the oscillation can be noticed. At the maximum excitation frequency under consideration (Fig. 10i, f=230 Hz), the C_n trace becomes more irregular again. In the C_n spectrum (Fig. 11i), only one peak of small amplitude is visible.

C_n traces and C_n frequency spectra for strong humid air (inlet humidity H=80%, right column in Fig. 10) show similar, but not identical behaviour. The amplitudes of C_n oscillation are, in general, smaller then for dry air. This can indicate that the range of motion of the separation point is now smaller. The most important observation is that at low excitation frequency (n_e=0.04) no components corresponding to the buffet are visible in the spectrum (Fig. 11b). This is due to the suppression of separation point oscillations in the case of humid air.

RMS values of the C_n pulsations for various air humidity under consideration are shown in detail in Fig. 12 versus excitation number n_e. For dry air (inlet humidity H=12%), a maximum of the C_n oscillation is noticed at excitation frequency close to the buffet frequency (n_e=0.82). The RMS level is very high ($C_n'_{RMS}$=0.23). With increasing or decreasing excitation frequency, the pulsation of C_n decreases, but is still very high. At the lowest and highest excitation frequencies under consideration (n_e =0.04 and n_e =0.12), $C_n'_{RMS}$ takes values of 0.14 and 0.11, respectively.

By increasing the air humidity, the extreme $C_n'_{RMS}$ values decrease from 0.22 at inlet humidity H=40% to 0.17 for humid air (inlet humidity H=60% and 80%). At the same time, the excitation frequency corresponding to these extreme values diminishes to the value n_e =0.7. This seems to be connected, as before, with the stabilisation of the buffet phenomenon by the humid air.

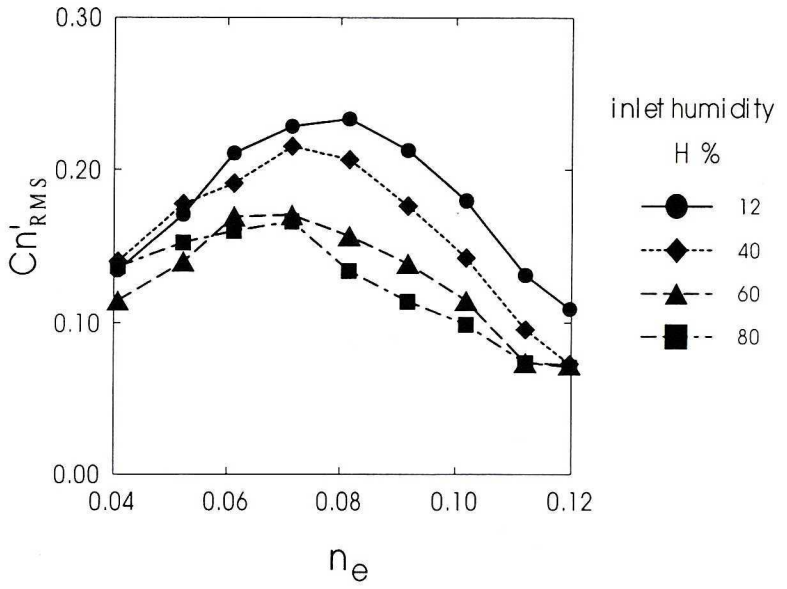

Fig. 12 RMS values of C_n pulsations versus excitation parameter for different air humidity values

4. Conclusions

The transonic airfoil flow is very sensible to background flow oscillations. They cause the motion of the shock wave in a wide displacement range and, in consequence, variation of momentary pressure distribution, especially on the upper airfoil surface.

The unsteady flow characteristics depend, first of all, on the excitation frequency. Extreme amplitudes of the normal force occur at frequencies typical for self-existing airfoil oscillations (n_e=0.08). The normal force variations diminish when the excitation frequency differs from this value. At frequencies considerably lower than the buffet frequency, two different oscillations occur on the airfoil at the same time.

With an increase of air humidity, the normal force variations considerably decrease, up to 40% in the case of maximum humidity under consideration. In addition, the excitation frequency corresponding to the value of maximum force variations decreases with an increase in the air humidity.

This work has been supported by State Commitee for Scientific Research in Poland (Project No 7 T07A 026 16).

Manuscript received by Editorial Board, September 07, 2001;

REFERENCES

[1] Mabey D.G.: Physical phenomena assotiated with unsteady transonic flows, in Unsteady transonic aerodynamics, ed. D. Nixon, Progress in Astronautics and Aeronautics, Vol. 120, 1989, pp. 1÷56.

[2] Levy L.L.: Experimental and computational steady and unsteady transonic flows about a thick airfoil. AIAA Journal, Vol. 16, 1978, pp. 564÷572.

[3] Levy L.L., Bailey H.E.: Computation of airfoil buffet boundaries. AIAA Journal, Vol. 19, 1981, pp.1488÷1490.

[4] Huang X.Z.: Transonic buffet of a supercritical airfoil, RTO–TR 26, 2000, pp. 319÷339.

[5] Lee B. H. K.: Oscillatory shock motion caused by transonic shock boundary-layer interaction. AIAA Journal, Vol. 28, 1990, No. 5, pp. 942÷944.

[6] Dor J. B.: Mignosi A., Seraudie A., Benoit B.: Wind tunnel studies of natural shock wave-separation instabilities, for transonic airfoil tests. IUTAM Symposium Transonicum III, 1988, DFVLR-AVA Göttingen.

[7] Geissler W.: Verfahren in instationären Aerodynamic, DLR Göttingen, Rep 93-21, 1993.

[8] Mabey D.G.: Some aspects of aircraft dynamic loads due to flow separation. Progr. Aerospace Sci. 26, 1989, pp. 115÷151.

[9] Fradenburgh E.A.: Basic aerodynamics for rotor performance, Paper 2 in AGARD Raport No.781, 1990.

[10] Vuillet A: Rotor and blade aerodynamic design, Paper 3 in AGARD Raport No.781, 1990.

[11] JohnsonW.: Airloads, wakes and aeroelasticity, Paper 6 in AGARD Raport No.781, 1990.

[12] Davis S.S., Malcolm G.N.: Transonic shock- wave, boundary- layer interactions on an oscillating airfoil, AIAA J. Vol. 18, No.11, 1980, pp. 1306÷1312.

[13] Chyn W.J., Davis S.S.: Numerical studies of unsteady transonic flow over an oscillating airfoil, AGARD–374, Paper 3 1984.

[14] Triebstein H., Voss R.: Transonic pressure distribution on a two- dimentional 0012 and supercritical MBB-A3 profile oscillating in heave and pitch, AGARD–374, Paper 2, 1984.

[15] Ahmed S., Chandrasekhara M.S.: Reattachmed studies of an oscillating airfoil dynamic stall flowfield. AIAA J. Vol.32, No. 5, 1994, pp. 1006÷1012.

[16] Wernet P., Geissler W., Raffel M., Kompenhans J.: Experimental and numerical investigations of dynamic stall on a pitching airfoil. AIAA J. Vol. 34, No.5, 1996, pp. 982÷989.

[17] Ruyck J. de. Thirsch Ch.: Velocity and turbulence measurments in dynamically stalled boundary Layers on an oscillating airfoil, Paper 4, AGARD–CP No. 386, 1985.

[18] Houwink R.: Unsteady airload computations for airfoils oscillating in attached and separated compressible flow, Paper 14, AGARD–CP–386, 1985.

[19] Szumowski A.P., Meier G.E.A.: Forced oscillations of airfoil flows. Experiments in Fluids 21, 1996, pp. 457÷464.

[20] Selerowicz W.C., Szumowski A.P.: Airfoil flow instabilities induced by background flow oscillations. Experiments in Fluids, 2002 (in print).

Wpływ wilgotności powietrza na oscylacyjny opływ profilu

Streszczenie

W pracy badano na drodze eksperymentalnej wpływ wilgotności powietrza na oscylacyjny opływ profilu NACA 0012 przy liczbie Macha M=0.71 i kącie natarcia α=8.5°. Oscylacje przepływu głównego były generowane przez obracającą się płytkę, umieszczoną za profilem. Częstotliwości oscylacji obejmowały zakres od 0.5 do 1.5 częstotliwości buffetu. Prezentowane wyniki pokazują, że zmiany składowej normalnej siły aerodynamicznej zależą silnie od częstotliwości wymuszającej i osiągają wartości maksymalne dla częstotliwości typowych dla buffetu. Wzrost wilgotności powietrza prowadzi do znacznego zmniejszenia zmian siły aerodynamicznej.